Published online 27 October 2012 *Nucleic Acids Research, 2013, Vol. 41, No. 1* ***327–339***
doi:10.1093/nar/gks970

Cross-talk between prion protein and quadruplex-forming nucleic acids: a dynamic complex formation

Paola Cavaliere[1], Bruno Pagano[2], Vincenzo Granata[3], Stephanie Prigent[4], Human Rezaei[4], Concetta Giancola[5,*] and Adriana Zagari[1,3,*]

[1]Dipartimento delle Scienze Biologiche, Università degli Studi di Napoli ''Federico II'', Naples 80134, [2]Dipartimento di Chimica Farmaceutica e Tossicologica, Università degli Studi di Napoli ''Federico II'', [3]CEINGE, Biotecnologie Avanzate S.c.a r.l., Naples 80131, Italy, [4]Virologie et Immunologie Moléculaires Equipe Biologie Physico-chimique des Prions, Institut National de la Recherche Agronomique (INRA), Jouy-en-Josas 78350, France and [5]Dipartimento di Scienze Chimiche, Università degli Studi di Napoli ''Federico II'', Naples 80126, Italy

Received March 21, 2012; Revised September 19, 2012; Accepted September 25, 2012

ABSTRACT

Prion protein (PrP) is involved in lethal neurodegenerative diseases, and many issues remain unclear about its physio-pathological role. Quadruplex-forming nucleic acids (NAs) have been found to specifically bind to both PrP cellular and pathological isoforms. To clarify the relevance of these interactions, thermodynamic, kinetic and structural studies have been performed, using isothermal titration calorimetry, surface plasmon resonance and circular dichroism methodologies. Three quadruplex-forming sequences, d(TGGGGT), r(GGA GGAGGAGGA), d(GGAGGAGGAGGA), and various forms of PrP were selected for this study. Our results showed that these quadruplexes exhibit a high affinity and specificity toward PrP, with K_D values within the range 62÷630 nM, and a weaker affinity toward a PrP-β oligomer, which mimics the pathological isoform. We demonstrated that the NA quadruplex architecture is the structural determinant for the recognition by both PrP isoforms. Furthermore, we spotted both PrP N-terminal and C-terminal domains as the binding regions involved in the interaction with DNA/RNAs, using several PrP truncated forms. Interestingly, a reciprocally induced structure loss was observed upon PrP–NA interaction. Our results allowed to surmise a quadruplex unwinding-activity of PrP, that may have a feedback *in vivo*.

INTRODUCTION

The concept that a protein can be the causative agent for transmissible diseases challenged the traditional knowledge that transmission results solely from an agent that carries genetic information. This new paradigm was brought by cellular prion protein (PrP^C), which is involved in a rare but fatal family of neurodegenerative disorders that affect humans and animals. Prion diseases, in addition to sporadic and inherited forms, may be acquired by transmission of an infectious agent. Accordingly to the 'protein only' hypothesis, the infectious agent is a self-perpetuating conformer of prion protein (PrP), namely PrP^{Sc}, capable of transmitting and replicating its 'wicked' conformation (1,2). Indeed PrP^C, which possesses a high α-helix content, is converted in the β-rich insoluble conformer PrP^{Sc}. This form acts as a template for PrP^C to induce misfolding and then generating more PrP^{Sc}. How this conversion occurs is not yet elucidated but all proposed mechanisms include a formation of soluble β-oligomers, that are neurotoxic species. The 'protein only' hypothesis excluded the participation of nucleic acids (NAs) in prion propagation. However, several groups have suggested that an additional, as yet unknown, factor—including NA—might initiate or modulate the PrP^C to PrP^{Sc} conversion (3–5).

Similarly to other proteins associated to neurodegeneration, PrP has been found in the cytosol (6) and in the nucleus as well (7–11). Having a common place to cross-talk, NAs do actually form an interesting group of PrP molecular partners. Indeed, it was shown that PrP can bind small NAs *in vitro* with nanomolar affinity (3,4,12) and these interactions can lead to conformational changes

*To whom correspondence should be addressed. Tel: +39 081 3737913; Fax: +39 081 3737808; Email: adriana.zagari@unina.it
Correspondence may also be addressed to Concetta Giancola. Tel: +39 081 674266; Fax: +39 081 674090; Email: concetta.giancola@unina.it
Present address:
Paola Cavaliere, Unité de Génétique Moléculaire, Institut Pasteur, 75724 Paris Cedex 15, France.

of the protein (3,4,12,13), suggesting a physiological role of PrP as an NA-binding protein (14–18). Furthermore, NAs have been used to create *de novo* synthetic prion and therefore have been proposed as the lacking cofactors that might facilitate the PrP transconformation *in vivo* (19,20).

Many studies have been devoted to the selection of RNA and/or DNA molecules able to specifically bind to both PrP^C and its β-rich isoform (12,21–25). Moreover, many works have highlighted the relevance of specific features possessed by NAs for a high-affinity binding with PrP. In particular, some of them were shown to contain a shared sequence and fold, i.e. contiguous guanine repeats and quadruplex structures (21,23,25,26).

In a previous work, RNA aptamers against recombinant bovine PrP and its amyloidogenic β isoform were obtained by means of SELEX method (23). Interestingly, all selected aptamers contained a core of four GGA tandem repeats. The authors found that the RNA 12-mer, $r(GGA)_4$, is the minimal sequence required to keep a high-affinity binding toward both PrP isoforms (23). This RNA r(GGAGGAGGAGGA) (R12) forms an intramolecular parallel quadruplex with a standard G-tetrad plane and an unusual G(:A):G:G(:A):G hexad one (21). Two R12 quadruplexes form a dimer in a tail-to-tail manner through hexad–hexad stacking (Figure 1A). The R12 structure shares common features with the one formed by its DNA counterpart d(GGAGG AGGAGGA) (D12). Indeed, two D12 quadruplexes form a dimer composed of two G-tetrad and two G(:A):G(:A):G(:A):G heptad planes (Figure 1B) (27). As for R12, each monomer of D12 forms an intramolecular parallel quadruplex. D12 is one of the few DNA oligonucleotides showed to form an intramolecular parallel quadruplex. The unique conformation of the GGA segments seems to be indispensable for the formation of the dimeric parallel quadruplex structure, which is largely stabilized by the base-stacking interactions (28). It is worth noting that GGA triplet repeats, potentially able to fold into G-quadruplexes, are also widely present among eukaryotic genomes, being found in portion of humans and mouse cellular DNA and within gene regulatory regions and recombination hot spot sites (29).

Indeed, the biological relevance of quadruplex structures is supported by the occurrence of G-rich sequences, able to adopt this peculiar fold, in genomic regions adjacent to transcriptional sites and in telomeres (30–32). The truncated telomeric sequence from *Oxytricha* and *Tetrahymena* telomeric DNA, d(TGGGGT), has been previously reported to form a tetramolecular parallel-stranded guanine-quadruplex, $[d(TGGGGT)]_4$, with four G-tetrad planes (Figure 1C) (33). Investigations on binding between this short natural sequence and PrP has never been done so far, even though it can be considered a good model to get insights into the possible role of quadruplex-forming NAs for prion biology. In fact, the lack of loops connecting the strands may provide information on the molecular basis of recognition with the G-tetrads core.

Despite all the efforts aimed at clarifying the interaction between PrP and NAs, enduring questions remain about (i) the RNA/DNA molecular recognition; (ii) the structural stability of the components; (iii) the thermodynamics and the kinetics of the binding process; and (iv) the possible functional significance of the interaction. In this article, we have selected the three quadruplex-forming NAs: d(TGGGGT), R12 and D12, to perform a thermodynamic, kinetic and structural study of their interaction with ovine PrP, by employing biophysical methodologies. We have considered a self-consistent set of three parallel quadruplexes, embodying an (i) RNA sequence and its (ii) DNA counterpart to evaluate, if any, the difference between RNA and DNA, and the (iii) $[d(TGGGGT)]_4$ to evaluate the role of a simple G-tetrad scaffold, independently of loops, hexad or heptad planes.

Our findings showed, through a detailed quantitative analysis, that all the quadruplex-forming RNA and DNA here examined exhibit a high affinity toward ovine PrP and a weaker affinity toward the β-rich PrP oligomer, which mimics the features of the PrP^{Sc} pathological isoform. Moreover, using the 'Dickerson duplex', that is formed from the self-complementary sequence d(CGCGA ATTCGCG), we showed that the binding to quadruplex is selective over this widely used duplex model. We therefore identified the quadruplex architecture, adopted by the three NA sequences, as the structural determinant for the RNA/DNA recognition by PrP. Interestingly, we observed that a remarkable structural modification of both interacting partners is a typical feature of PrP–NAs binding. Collectively, our results allowed to put forward a quadruplex unwinding-activity of PrP, in which each domain of the protein plays distinct functional roles.

MATERIALS AND METHODS

Protein production and materials

The full-length ovine PrP (flPrP) (A^{136} R^{154} Q^{171} variant, 23–234) and the truncated forms, ΔPrP (103–234) and ΔPrP (124–234), were produced in *Escherichia coli* and purified as previously described (34). The buffer used to desalt the proteins, on a HiPrep desalting column, was MES 15 mM pH 6.0, KCl 70 mM. Final protein concentration was measured by optical density at 280 nm using an extinction coefficient of 58 718 $M^{-1}cm^{-1}$ for the flPrP and 180 05 $M^{-1}cm^{-1}$ for both the ΔPrP forms, deduced from the aminoacid sequence.

The generation of oligomers from ovine flPrP was performed by dissolving the protein in a solution of HCl 0.1 M, pH 1.0. The solution, at a final concentration of 80 μM, was incubated for 12 h at 25°C. The samples were cooled down to 15°C and eluted with sodium citrate 20 mM, pH 3.4 on a TSK 4000SW (60 cm × 0.78 cm) column using an Akta FPLC chromatography equipment (GE Healthcare). The oligomeric PrP form collected, elutes at 12.5 ml, which corresponds to O1 oligomer (36-mer), accordingly to previous results (35). Homogeneous fractions of the oligomer were collected.

NAs were purchased from PRIMM (Milan) and purified by standard methods. The samples were prepared by dissolving the lyophilized compound in MES 15 mM pH 6.0, KCl 70 mM. The solutions have been annealed by

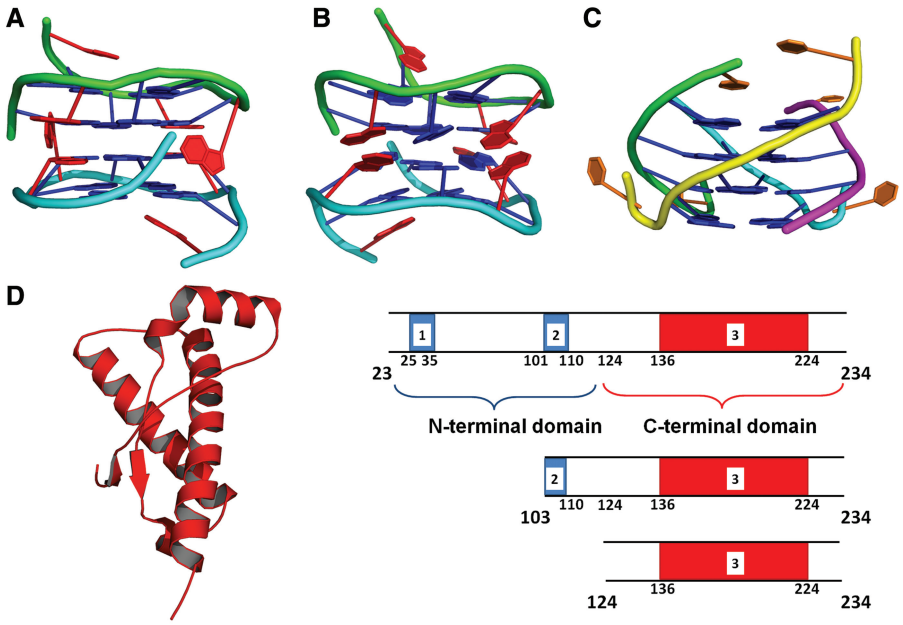

Figure 1. The player molecules. Cartoon of (**A**) the dimeric architecture of R12 (PDB code 2rqj (21)) and (**B**) D12 (PDB code 1MYQ (27)) quadruplexes in which each strand is drawn in green and cyan (guanines are in blue, adenines in red and thymines in orange). The hexad planes, in R12, and the heptad planes, in D12, lie at the dimer interface; (**C**) the tetramolecular G-quadruplex $[d(TGGGGT)]_4$ (PDB code 244D, (33)) in which the four strands are colored in yellow, magenta, cyan and green. (**D**) Ribbon representation of the PrP C-terminus structure, along with the schematic representation of flPrP (23–234), $\Delta PrP_{103–234}$ and $\Delta PrP_{124–234}$. The regions in the sequence depicted in blue correspond to the putative NAs-binding sites of PrP located in the N-terminal domain (18,22), and the region depicted in red corresponds to the NAs-binding site located in the C-terminal domain (18,38).

heating at 95°C for 5 min and slowly cooling to room temperature. The concentration of the dissolved oligonucleotide has been evaluated by UV measurement at 95°C, using molar extinction coefficient of 57 800 $M^{-1} cm^{-1}$ for d(TGGGGT), 110 700 $M^{-1} cm^{-1}$ for d(CGCGAATTCGCG) and 135 500 $M^{-1} cm^{-1}$ for both r(GGAGGAGGAGGA) and d(GGAGGAGGAGGA), calculated by the nearest-neighbor model (36). Native gel electrophoresis was performed to verify the conformational homogeneity of G-quadruplex species (Supplementary Methods and Supplementary Figure S1). In all experiments, R12 and D12 concentration was referred to quadruplex dimers, apart from $[d(TGGGGT)]_4$ for which concentration was referred to a single tetramolecular quadruplex. The unfolded $[d(TGGGGT)]_4$, R12 and D12 were obtained by removing K^+ ions from the solution through dialysis against either MES 15 mM pH 6.0 or MES 15 mM pH 6.0, LiCl 70 mM. Dialysis was performed for 24 h, a time longer with respect to the kinetics of tetramolecular quadruplex-folding/unfolding processes. The unfolded state of dialyzed NAs solutions was assessed by recording CD spectra in the 320 ÷ 200 nm interval.

Isothermal titration calorimetry

Isothermal titration calorimetry (ITC) experiments were carried out at 25°C using a high-sensitivity CSC-5300 Nano-ITC microcalorimeter from Calorimetry Science Corporation (Lindon, Utah) with a cell volume of 1 ml. Only after reaching the baseline stability, the experiments were performed. In each titration experiment, volumes of 10 µl of a solution containing $[d(TGGGGT)]_4$, R12 or D12 at a concentration within the range 80 ÷ 130 µM were injected into a PrP-containing solution in the same buffer (MES 15 mM pH 6.0, KCl 70 mM), using a computer-controlled 250 µl microsyringe. In the case of ITC titration carried out with the unfolded D12, both the aptamer and PrP were in the same buffer MES 15 mM, pH 6.0. All the PrP forms were prepared at a concentration of 16 µM. In order to allow the system to reach the equilibrium, we applied a time interval of 300 or 400 s between each injection. Heat produced by NAs dilution was evaluated by performing a control experiment, titrating each NA into the buffer alone. The heat of interaction (enthalpy change, ΔH) was calculated after correction for the heat of NA dilution. The corrected heat values were plotted as a function of the NA:PrP molar ratio, to estimate the stoichiometry of interaction (n) (37).

Surface plasmon resonance

Surface plasmon resonance (SPR) experiments were performed using a Biacore T200 system (GE Healthcare, Uppsala, Sweden), at 25°C. flPrP, the truncated PrP forms and the PrP-β oligomer were immobilized on a CM5 (research grade) by the standard amine coupling procedure, using HBS-EP buffer (HEPES 10 mM, NaCl 150 mM, EDTA 3 mM, 0.005% Surfactant P20, pH 7.4) as running buffer. The PrP forms were immobilized through activation of the sensor chip with 60 µl of N-hydroxysuccinimide (NHS) and N-ethyl-N-(dimethylaminopropyl)-carbodiimide (EDC) at 10 µl min^{-1}, followed by 30 µl injection of PrP forms diluted in 10 mM sodium

acetate buffer pH 5.0. Unreacted activated groups were blocked by a 60 µl injection of 1 M ethanolamine at 10 µl min^{-1}. Final PrP immobilized levels were typically between ~3500 and 4300 RU, corresponding to a protein concentrations of 35 ÷ 43 mg ml^{-1} on the surface layer. Subsequently, [d(TGGGGT)]$_4$, R12, D12 and Dickerson duplex were injected as analytes at various concentrations (from 50 nM to 50 µM), and using MES 15 mM pH 6.0, KCl 70 mM as running buffer. The binding assays were performed under various conditions: (i) contact time of 60, 120 and 360 s and dissociation time of 180, 240, 300 and 480 s to evaluate the best kinetic model; (ii) flow rate of 30 and 60 µl min^{-1} to evaluate the contribution of mass transport. Analogously, SPR experiments with the unfolded [d(TGGGGT)]$_4$, R12 and D12, were carried out injecting the analytes at various concentrations (from 50 nM to 50 µM), at a contact time of 120 s, dissociation time of 300 s and flow rate of 30 µl min^{-1} and using either MES 15 mM pH 6.0 or MES 15 mM pH 6.0 70 mM LiCl as running buffers.

For all SPR experiments, the chip was regenerated by removing bound analytes using the mobile phase $MgCl_2$ 0.25 M, injected for 30 s at 30 µl min^{-1}, after the analyte injection. Data were corrected using a blank sensor chip as control. Moreover, binding experiments were repeated using an excess of PrP in the mobile phase to avoid the re-binding during the dissociation step, and no difference was observed.

The SPR sensorgrams for each protein–NA interaction were analysed by curve-fitting using Biacore T200 Evaluation software provided with the Biacore device. Dose response curves were plotted using the SPR sensorgrams obtained in the conditions indicated in Figure 3 caption.

Various reaction models were applied to perform complete kinetic analysis of the sensorgrams, and the best fitting was considered in such a way that the χ^2 value, representing the statistical closeness of curve-fitting, became the lowest. The two-state reaction (conformation change) model was chosen, which is described as:

$$A + B \rightleftarrows AB \rightleftarrows AB^*$$

where A is the immobilized protein, B is the NA, AB represents the protein–NA complex and AB* represents the complex after the conformational change. The binding dissociation constant (K_D) was calculated from the equation:

$$K_D = \frac{k_{off1}}{k_{on1}} \times \frac{k_{off2}}{(k_{off2}+k_{on2})}$$

Circular dichroism

Circular dichroism (CD) spectra were recorded with a Jasco J-815 spectropolarimeter equipped with a Peltier type temperature control system (Model PTC-423S). CD measurements (190 ÷ 320 nm) were carried out in MES 15 mM pH 6.0 KCl, 70 mM at 20°C by using a 0.1 cm optical path length cell. CD titration was performed on the full-length and the truncated PrP forms, keeping constant the concentration of PrP (10 µM), and increasing the NA concentration up to a PrP:NA molar ratio of 1:2. Each solution of the mixture PrP–NA was prepared independently, without successive additions, to avoid complications due to dilution effects within titration experiments, and the spectra were recorded after few minutes upon addition of NAs. CD spectra, recorded with a time constant of 4 s, a 2 nm band width, and a scan rate of 20 nm min^{-1}, were signal-averaged over at least three scans. The baseline was corrected by subtracting the buffer spectrum. Melting curves of all NAs were also recorded (Supplementary Methods).

Transmission electron microscopy

TEM images were collected using a Zeiss EM902 (80 kV) microscope. Briefly, 10 µl of the samples were adsorbed onto carbon-coated Formvar grids (Agar Scientific). Then, each grid was washed three times with water, stained with 2% uranyl acetate and finally air-dried. All the samples were in MES 15 mM pH 6.0, KCl 70 mM. Since precipitation occurred as soon as the two partners are mixed, there was no incubation time to wait for.

RESULTS AND DISCUSSION

In order to get insights into kinetics, affinity and enthalpy change associated with ovine PrP binding to [d(TGGGGT)]$_4$, R12 and D12, we performed ITC and SPR experiments. Various PrP truncated forms, *ad hoc* designed, were produced to identify the regions involved in the interaction, as well as the forces that drive the complex formation. Indeed, three distinct PrP binding sites have been previously indentified for NAs: two lysine clusters (aa 25–34 and 101–110 in ovine PrP) located at the ends of the unstructured N-terminal domain (18,22), and a third site, located in the structured C-terminal domain, in which the amino acids involved are not yet well-established (18,38). Hence, in addition to flPrP (23–234), we investigated the interaction with the deleted proteins $\Delta PrP_{103–234}$ and $\Delta PrP_{124–234}$ that lack the first and both lysine clusters, respectively (Figure 1D).

Additionally, the binding with the pre-amyloid ovine PrP-β oligomer, that mimics the early stage of PrP^{Sc} formation, was investigated by SPR. As ovine PrP produces a mixture of β-rich oligomers, we have selected the largest one, corresponding to 36-mer, which is the only precursor of amyloid-like fibrils (35).

Finally, in order to study the structural modifications that might be induced by the PrP–NA interactions, we performed CD experiments to monitor the changes in the secondary structures either of protein or NAs. To gain more information on the thermal stability of all studied NAs we have measured their melting temperature (Supplementary Figure S2).

Thermodynamic data from ITC titration

The resulting profiles obtained by ITC titrations of flPrP, $\Delta PrP_{103–234}$ and $\Delta PrP_{124–234}$ with [d(TGGGGT)]$_4$ are shown in Figure 2, as the representative ones. ITC data of all the PrP forms with R12 and D12 are shown in

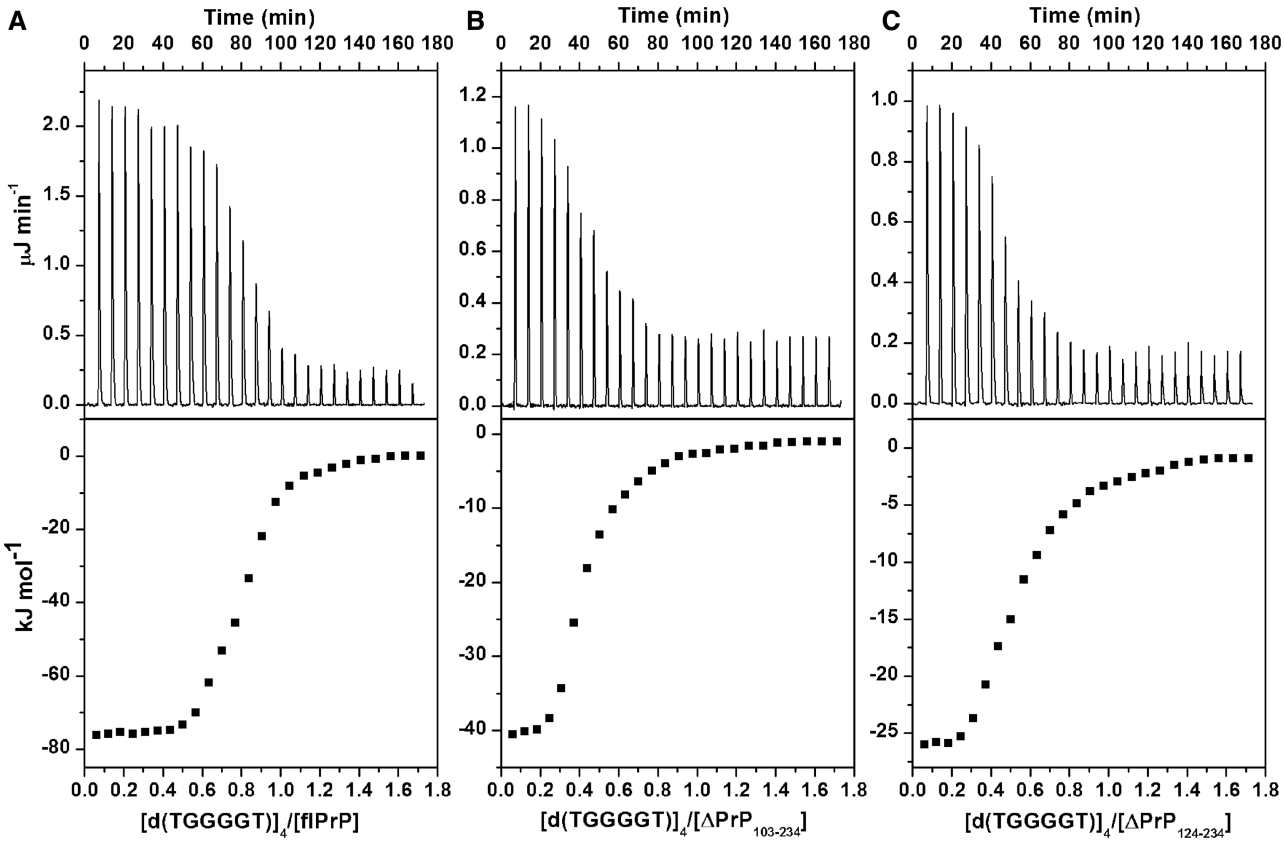

Figure 2. ITC data obtained for the interaction of $[d(TGGGGT)]_4$ with (**A**) flPrP, (**B**) $\Delta PrP_{103\text{-}234}$ and (**C**) $\Delta PrP_{124\text{-}234}$. In each panel, ITC raw profile (at the top) and integrated heat values plotted as a function of the molar ratio (at the bottom) are shown.

Supplementary Figure S3, with the exception of the flPrP-D12 system, since precipitation at the end of ITC experiments precluded any further analysis. In particular, ITC profiles along with the integrated heat data are shown for all the system studied, apart from $\Delta PrP_{124\text{–}234}$-R12, for which only the raw ITC profile is shown, since no binding was detected (Supplementary Figure S3C). In all figures, the heat values were plotted as a function of the NA:PrP molar ratio to estimate, from the inflection point, the stoichiometry of interaction. In the plot, both R12 and D12 aptamers were considered to be a quadruplex dimer, while $[d(TGGGGT)]_4$ was considered as a single tetramolecular quadruplex. The data suggested that the stoichiometry relative to the interaction of $[d(TGGGGT)]_4$, R12 and D12 with the truncated PrP forms resulted to be 1:0.5 (ratio of PrP *per* NA), whereas the stoichiometry obtained for the interaction of $[d(TGGGGT)]_4$ and R12 with flPrP was 1:1. Since during the binding events a concomitant conformational change of reactants occurs (see below), we choose not to fit the ITC data to a model, as no appropriate fitting model is currently available to adequately describe the data (two-step binding reaction model in which ligand binding is coupled to a conformational transition). The values are reported in Table 1 and represent the total, model free, enthalpy change for the process, and indicate that, in all cases, the overall processes are enthalpically favorites.

Table 1. Stoichiometry and enthalpy change for the interaction of flPrP, $\Delta PrP_{103\text{–}234}$ and $\Delta PrP_{124\text{–}234}$ with $[d(TGGGGT)]_4$, R12 and D12, determined by ITC at 25°C

PrP-NA interaction	*n*	ΔH (kJ mol^{-1})
flPrP-$[d(TGGGGT)]_4$	1.1 ± 0.1	−76.4 ± 1.0
$\Delta PrP_{103\text{–}234}$-$[d(TGGGGT)]_4$	0.5 ± 0.2	−40.5 ± 1.0
$\Delta PrP_{124\text{–}234}$-$[d(TGGGGT)]_4$	0.5 ± 0.2	−26.2 ± 1.0
flPrP-R12	0.9 ± 0.1	−81.6 ± 1.0
$\Delta PrP_{103\text{–}234}$-R12	0.5 ± 0.2	−68.4 ± 1.0
$\Delta PrP_{124\text{–}234}$-R12	NB	NB
flPrP-D12	ND	ND
$\Delta PrP_{103\text{–}234}$-D12	0.5 ± 0.2	−86.2 ± 2.0
$\Delta PrP_{124\text{–}234}$-D12	0.5 ± 0.2	−17.6 ± 1.0

ND, not determined; NB, no binding detected.

In order to evaluate a possible interaction with single-stranded NAs and to confirm the PrP specificity toward the quadruplex structure, D12 was unfolded by removing K^+ ions from the solution, and ITC titration was performed using $\Delta PrP_{103\text{–}234}$, to avoid difficulties due to precipitation with the full-length protein. The heat changes obtained upon addition of the unfolded single-stranded D12 correspond to the heat of NA dilution (Supplementary Figure S4), demonstrating that PrP does not bind to unfolded RNA/DNA molecules lacking the quadruplex structure.

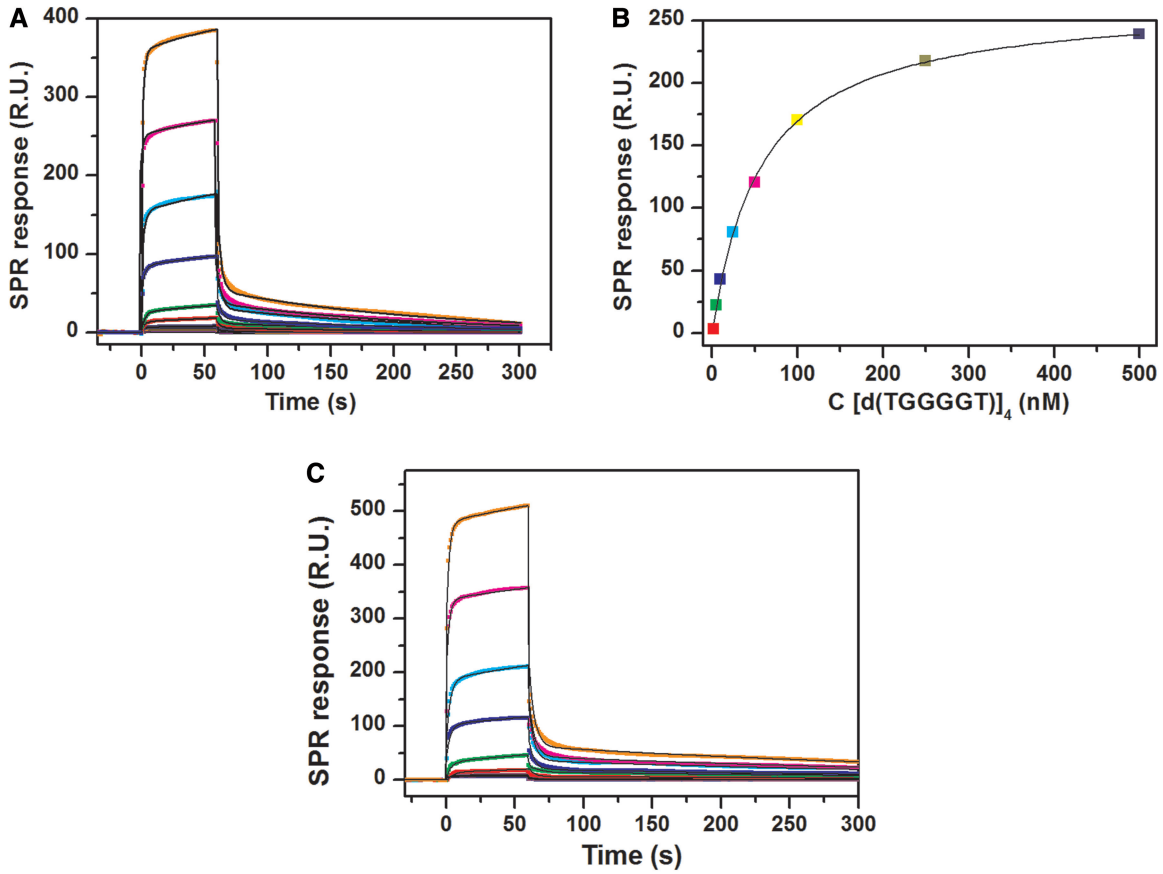

Figure 3. (**A**) Time evolution SPR sensorgrams related to the interaction with flPrP, obtained at various concentrations of $[d(TGGGGT)]_4$ and at a contact time of 60 s, a dissociation time of 240 s and a flow rate of 60 µl min^{-1}. SPR sensorgrams are reported with the corresponding fit (dot lines), based on the two-state reaction model which includes a conformational change. (**B**) Dose response curve obtained for the interaction between flPrP and $[d(TGGGGT)]_4$, at a contact time of 360 s, a dissociation time of 480 s and at a flow rate of 30 µl min^{-1}. (**C**) SPR sensorgrams of the PrP-β interaction with $[d(TGGGGT)]_4$ obtained under the same conditions as in (A).

Kinetic and binding data from SPR experiments

To get insights into the kinetics and the affinity of these interactions, SPR experiments were performed on the same systems used in ITC titrations. In addition, (i) the beta structured PrP oligomer, PrP-β, that mimics the scrapie infective form, has been used to verify whether this pathological-like PrP form participates in the binding; and (ii) the Dickerson duplex has been used to assess the specificify of the PrP toward quadruplex-forming NAs. SPR sensorgrams obtained for the interaction of flPrP with $[d(TGGGGT)]_4$ are shown in Figure 3A, as example, whereas SPR data of the other systems are shown in Supplementary Figure S5. Since the kinetic and binding constants were independent of the experimental conditions, SPR reported sensorgrams are those obtained at the lowest contact time, at a dissociation time of 240 s and at the highest flow rate (See Materials and Methods section).

Experimental SPR data were fitted using various models and on the basis of χ^2 values and CD results (see below), the two-step binding reaction model, that takes into account a conformational change of one or both components upon complex formation, was chosen as the best representative of the studied PrP–NAs interactions. The association (k_{on1}, k_{on2}) and dissociation rate constants (k_{off1}, k_{off2}) of the two reaction steps were derived from the fitting and the binding dissociation constants (K_D) were kinetically determined (Table 2). For the systems studied, the dose response curves were obtained by plotting the maximum SPR signal against NA concentration (Figure 3B). In all cases, the curves reached a final plateau, indicating that all binding sites have been saturated and no aspecific binding has occurred.

In details, k_{on1} values were greater for the interaction of all the NAs with flPrP with respect to the values obtained for the interaction with both $\Delta PrP_{103–234}$ and $\Delta PrP_{124–234}$. On the other hand, k_{off2} values are very similar among all the systems, suggesting that the dissociation phase does not depend on the binding of NAs to the unstructured PrP N-terminal domain. Interestingly, the fast dissociation process occurring upon recognition and binding suggests that the formed complexes are dynamic. This is in line with the fact that PrP–NA complexes have never been isolated so far, and NMR studies (18,39) did not result in a well-defined structure of the complex, or in that of the NA within the complex; only some changes in PrP structure were revealed. A reliable hypothesis is that other

Table 2. Kinetic and binding parameters for the interaction of flPrP, $\Delta PrP_{103–234}$, $\Delta PrP_{124–234}$ and PrP-β oligomer with $[d(TGGGGT)]_4$, R12 and D12, determined by SPR. Data relative to flPrP-Dickerson duplex determined by SPR

PrP-NA interaction	k_{on1} ($\times 10^3 M^{-1} s^{v1}$)	k_{off1} ($\times 10^{-1} s^{-1}$)	k_{on2} ($\times 10^{-2} s^{-1}$)	k_{off2} ($\times 10^{-3} s^{-1}$)	K_D ($\times 10^{-6}$ M)[a]
flPrP-$[d(TGGGGT)]_4$	38 ± 2	1.6 ± 0.1	1.7 ± 0.1	2.9 ± 0.2	0.63 ± 0.02
$\Delta PrP_{103–234}$- $[d(TGGGGT)]_4$	19 ± 2	1.8 ± 0.2	1.9 ± 0.1	14 ± 1	4.0 ± 0.2
$\Delta PrP_{124–234}$-$[d(TGGGGT)]_4$	3.0 ± 0.2	1.7 ± 0.1	0.74 ± 0.02	5.0 ± 0.1	18 ± 2
flPrP-R12	81 ± 3	0.39 ± 0.02	6.5 ± 0.1	1.14 ± 0.03	0.075 ± 0.002
$\Delta PrP_{103–234}$-R12	16.9 ± 0.4	1.66 ± 0.05	5.41 ± 0.06	1.17 ± 0.03	0.21 ± 0.01
$\Delta PrP_{124–234}$-R12	27.3 ± 0.4	1.22 ± 0.04	5.48 ± 0.05	1.41 ± 0.04	0.22 ± 0.01
flPrP-D12	79 ± 1	1.6 ± 0.2	4.6 ± 0.1	1.4 ± 0.1	0.062 ± 0.002
$\Delta PrP_{103–234}$-D12	37 ± 1	1.9 ± 0.1	7.7 ± 0.2	1.7 ± 0.1	0.11 ± 0.02
$\Delta PrP_{124–234}$-D12	19 ± 4	2.0 ± 0.1	13 ± 2	1.9 ± 0.1	0.42 ± 0.04
PrP-β-$[d(TGGGGT)]_4$	4.9 ± 0.3	5.5 ± 0.1	0.72 ± 0.02	0.84 ± 0.06	24 ± 3
PrP-β-R12	6.1 ± 0.3	1.5 ± 0.1	2.8 ± 0.1	4.3 ± 0.1	3.2 ± 0.3
PrP-β-D12	0.21 ± 0.01	0.17 ± 0.02	0.74 ± 0.02	0.41 ± 0.02	4.1 ± 0.2
flPrP-Dickerson duplex	3.1 ± 0.3	0.20 ± 0.01	0.22 ± 0.01	7.5 ± 0.3	500 ± 0.03

[a]The values of K_D were kinetically determined.

cellular components may participate in a larger and more stable macromolecular complex, *in vivo*.

An increase of the K_D values was observed for the interactions with the truncated PrP forms. Surprisingly, SPR experiments revealed a binding also between R12 and $\Delta PrP_{124–234}$, in apparent contrast to the results obtained by ITC. The different result obtained by ITC could be explained considering that the enthalpic contribution due to the interactions established between R12 and the structured PrP C-terminal domain may be compensated by the opposite contribution of the PrP unfolding process, not allowing to measure a binding-related heat. This interpretation is supported by the ITC data obtained for the interaction of $\Delta PrP_{124–234}$ with $[d(TGGGGT)]_4$ and D12, that presented the highest enthalpy change values (−26.2 and −17.6 kJ mol^{-1}, respectively).

SPR has proved to be very advantageous also in the study of the interaction between flPrP and D12, for which no information was obtained by means of ITC, due to precipitation. Indeed, using SPR methodology, the binding reaction occurs in a solution-independent manner. The comparison of K_D obtained for both R12 and D12 with flPrP reveals very similar values. Therefore, these findings indicate a high-affinity binding (within the same order of magnitude) of D12 with flPrP, such as found for R12 aptamer. It is worth mentioning that our results are in contrast with previous work in which R12 interaction with bovine PrP resulted to be stronger than the one with D12 (23). However, this difference could be ascribed to the PrP species (bovine and ovine) considered, as well as to the different methodologies used.

We also evaluated the affinity of the quadruplex-forming NAs toward the beta structured PrP-β oligomer (Figure 3C and Supplementary Figure S6). Prior to use, a CD spectrum was recorded to confirm that the oligomer was in the β-rich structure (data not shown). From a kinetic point of view, the association phase of all the NAs with PrP-β is slower compared to the α-rich PrP isoform, whereas a similar dissociation phase is displayed with both PrP isoforms. Specifically, the association rate obtained for the interactions involving $[d(TGGGGT)]_4$ and R12, are very similar, but the dissociation rate for the PrP-β-$[d(TGGGGT)]_4$ system is slower compared to the PrP-β-R12 system. Differently, the association and dissociation rates referred to the interaction of PrP-β with R12, are higher than those related to the interaction with D12.

Regarding the binding affinity, all the NAs exhibited a similar decrease in the affinity toward PrP-β oligomeric species with respect to the biologically functional monomeric α-PrP isoform, in agreement with previous data obtained using bovine PrP (23). Indeed, the K_D value obtained for the interaction between $[d(TGGGGT)]_4$ and PrP-β is 38-fold higher with respect to the interaction between $[d(TGGGGT)]_4$ and the full-length α-PrP isoform. Similarly, R12 and D12 showed an affinity toward PrP-β over 40-fold and 70-fold lower than for the full-length α-PrP isoform, respectively. This is in line with the diverse molecular complexity of the two PrP isoforms. The α-rich PrP isoform is monomeric, whereas PrP-β is a high molecular mass oligomer of 36-mer. Within this molecular assembly, Lys clusters may be less exposed, resulting in a weaker interaction with NAs.

To confirm the specificity of PrP toward the quadruplex-forming NA, affinity measurements were carried out toward the 12-mer Dickerson duplex (same size and 33% G content); results are listed in Table 2, last row. For the flPrP-$[d(CGCGAATTCGCG)]_2$ interaction, K_D is significantly higher. In detail, K_D is 794-, 6667- and 8064-fold higher with respect to $[d(TGGGGT)]_4$, R12 and D12, respectively, assessing the specificity of flPrP toward the quadruplex over the Dickerson duplex.

Finally, SPR binding assays were performed to evaluate the binding of the flPrP as well as the PrP-β oligomer, with the unfolded single-stranded d(TGGGGT), r(GGAGGA GGAGGA) and d(GGAGGAGGAGGA) sequences (data not shown). Two sets of measurements were carried out with and without Li^+, because this cation does not affect the NAs quadruplex structure but its effect on PrP features is unknown. No binding was observed in the two sets of measurements, neither with the monomeric PrP forms, in good agreement with ITC data, nor with the PrP-β oligomer. All together our results fully demonstrate the specificity of PrP toward quadruplex

over duplex and single strands. In other words, NA quadruplex architecture is essential for the recognition by both 'healthy' and 'pathological' PrP isoforms.

Identification of the PrP binding sites. Possible modes of interaction

All the NAs here used interact with flPrP as well as with the truncated PrP forms, suggesting that the interactions involve the three binding sites located along the protein. For the $[d(TGGGGT)]_4$, a roughly comparison between the difference of ΔH° relative to the interaction with flPrP and $\Delta PrP_{103–234}$ ($\Delta\Delta H^\circ = -35.9\,kJ\,mol^{-1}$), as well as the difference of ΔH° relative to the interaction with $\Delta PrP_{103–234}$ and $\Delta PrP_{124–234}$ ($\Delta\Delta H^\circ = -14.3\,kJ\,mol^{-1}$), suggests a greater number of contacts with the first lysine cluster (25–34) compared to the second lysine cluster and to the C-terminal domain. On the other hand, the comparison of the ΔH° obtained for the interaction of R12 with flPrP and $\Delta PrP_{103–234}$ suggests the second lysine cluster (101–110) being the major binding site, since the difference between the enthalpy change values is rather small ($\Delta\Delta H^\circ = -13.2\,kJ\,mol^{-1}\,kcal$).

It is worth recalling that ITC data showed a binding of R12 with both flPrP and $\Delta PrP_{103–234,}$ but no binding was detected with $\Delta PrP_{124–234}$. Differently, SPR allowed to detect a specific binding also with the PrP C-terminal domain, $\Delta PrP_{124–234}$, in contrast with previous data in which the interaction with RNAs was found to involve only the PrP N-terminal domain, without any contribution of the structured C-terminal domain (13,16,39), which instead participates in the interaction with DNAs (18). Therefore, the use of different techniques allowed detecting and characterizing a binding, which could have been neglected, if investigated with a single approach.

Finally, speculations about a major PrP binding site for D12 are restricted since no thermodynamic data were obtained for the interaction with flPrP. However, SPR experiments revealed a high binding affinity with flPrP. Moreover, D12 showed to interact with both PrP truncated forms, even though the major binding sites should be the two lysine clusters located in the N-terminal domain. In fact, the ΔH° value derived for the system $\Delta PrP_{124–234}$-D12 is markedly higher than the one obtained for $\Delta PrP_{103–234}$-D12, indicating the formation of a considerably lower number of favorable interactions. As result, the selected PrP forms allowed to identify the binding sites on PrP.

Regarding the PrP–NAs binding mode, it is worth recalling that a stoichiometry ratio of 1:0.5 was found for all the interactions with the truncated PrP forms, whereas the interaction of flPrP with $[d(TGGGGT)]_4$ and R12, presents a stoichiometry of 1:1. These results indicate that the whole PrP is required to establish the specific binding with the quadruplex-forming sequences. Moreover, the enthalpy change values obtained for all the interactions suggest that, although the PrP structured C-terminal domain participates to the interaction, the two lysine clusters at the N-terminal domain are the major binding sites for the NAs. In particular, we can speculate that the binding mode may involve an interaction of the PrP N-terminal domain with the grooves of the quadruplexes through electrostatic interactions between the positive charges of the two lysine clusters and the negative charges of the phosphate groups, as supported by the highly negative enthalpy values obtained for the systems involving flPrP and $\Delta PrP_{103–234}$. On the other hand, the C-terminal domain may cooperate to the binding with further weaker interactions, since the ΔH° values related to the binding of $\Delta PrP_{124–234}$ (the structured PrP C-terminal domain) with both $[d(TGGGGT)]_4$ and D12 are higher compared to those obtained with flPrP and $\Delta PrP_{103–234}$.

Nevertheless, it is worth noting that the diverse affinity obtained for the NA sequences here studied toward PrP indicates that these NAs bind in a diverse mode, likely with a diverse orientation of the regions involved in the binding. Also the differences of ΔH° may reflect a diverse contribution of non-covalent bonds to the complex stability.

Structural analysis of the interaction between PrP and quadruplex-forming DNA/RNA

At a molecular level, upon binding, pronounced structural variations on PrP (3,4,12,13) and on NAs, such as annealing, bending or strand exchange (15,17,40) were previously reported. To evaluate whether PrP and/or the quadruplex-DNA/RNA molecules undergo structural changes upon interaction, CD titration experiments were carried out. In all cases the CD analysis revealed structural alterations of one or both partners, providing an experimental support to a two-steps mechanism for the complex formation, involving a conformational change. For each experiment, it was taken into account that $[d(TGGGGT)]_4$, D12 and R12 exhibit a significant CD signal in the wavelength range typical of the secondary structure of proteins (Supplementary Figure S7). Therefore, it was evaluated whether the CD spectrum, corresponding to the PrP–NA complex, overlaps with that of the NA alone.

$[d(TGGGGT)]_4$ binding to PrP

CD spectra related to the interaction of flPrP with $[d(TGGGGT)]_4$ showed a loss of secondary structure for both complex partners (Figure 4A). Although it was not possible to subtract the CD spectrum of $[d(TGGGGT)]_4$ alone from the one corresponding to the complex, the CD signal decrease, observed for the protein, at a PrP:$[d(TGGGGT)]_4$ molar ratio of 1:0.2, can be ascribed to an actual loss of protein secondary structure. Indeed, $[d(TGGGGT)]_4$ has a low CD signal at 209 nm at this concentration (Supplementary Figure S7A). Interestingly, the CD spectra corresponding to the G-quadruplex, upon interaction with PrP, exhibited a shift of the maximum from 264 nm to ~275 nm, and of the minimum from ~244 nm to 254 nm, consistent with the unstructured single-stranded DNA. A similar behavior was observed for the interaction of $\Delta PrP_{103–234}$ with $[d(TGGGGT)]_4$. Also in this case, both components lost secondary structure (Figure 4B), although the structural loss of $[d(TGGGGT)]_4$ is lower compared to the complete disruption of the G-quadruplex architecture found for the interaction with

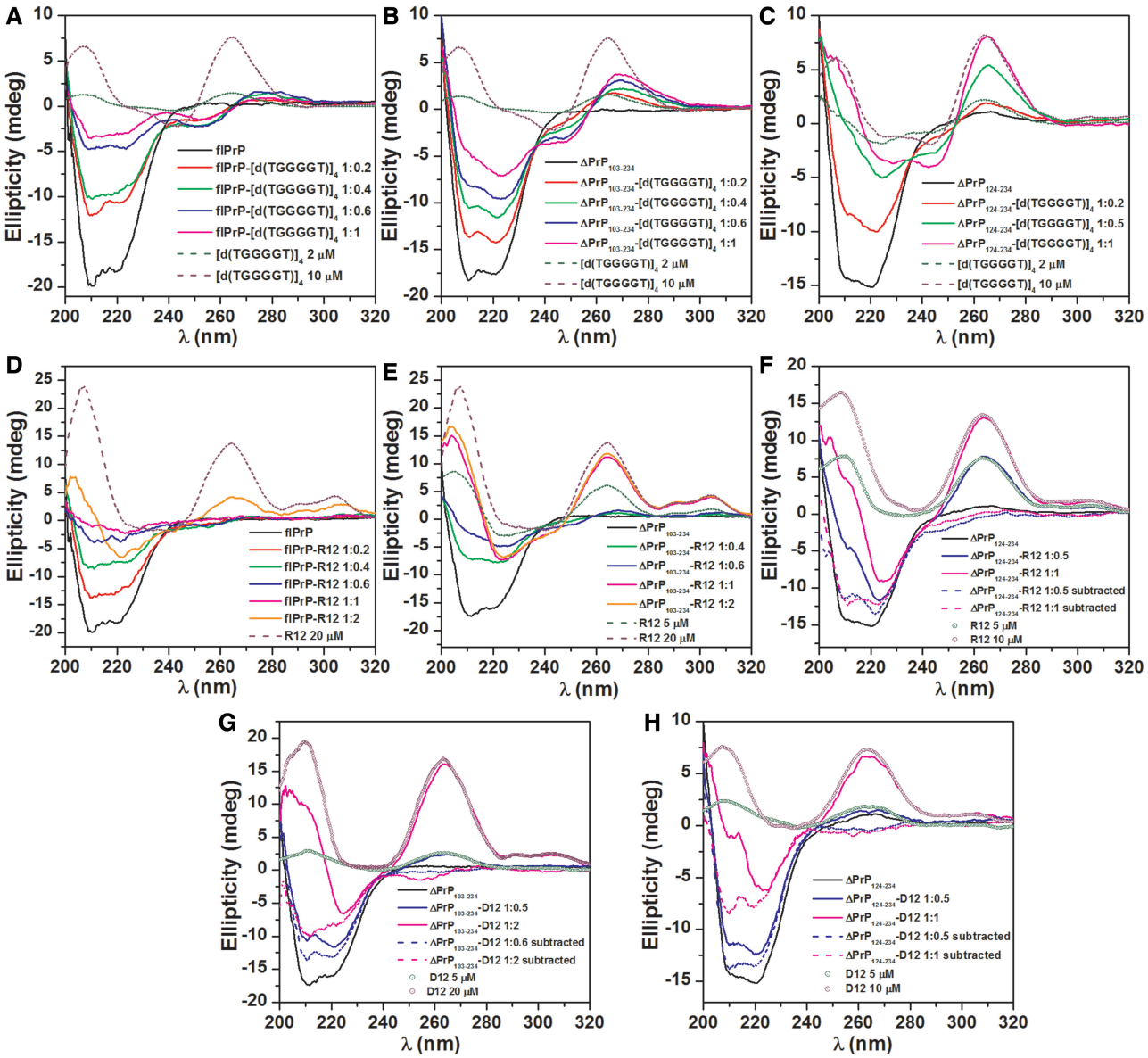

Figure 4. CD structural analysis of PrP interaction with $[d(TGGGGT)]_4$, R12 and D12. CD spectra recorded at various PrP:NAs molar ratios for the interaction of: $[d(TGGGGT)]_4$ with (**A**) flPrP, (**B**) $\Delta PrP_{103–234}$ and (**C**) $\Delta PrP_{124–234}$; R12 with (**D**) flPrP, (**E**) $\Delta PrP_{103–234}$ and (**F**) $\Delta PrP_{124–234}$; D12 with (**G**) $\Delta PrP_{103–234}$ and (**H**) $\Delta PrP_{124–234}$. In all panels the CD spectra of the NAs alone are also shown. In panels (F–H), CD spectra corresponding to the complex obtained by subtracting the CD spectra of the NA alone are shown.

flPrP. Finally, the binding with $\Delta PrP_{124–234}$ revealed no structural variations on the G-quadruplex fold of [d(TGGGGT)]$_4$, whereas the protein partially lost α-helical content (Figure 4C).

R12 binding to PrP

Also in this case, the CD structural analysis of the interaction with flPrP showed a loss of secondary structure for both interacting partners (Figure 4D). Analogously to [d(TGGGGT)]$_4$, the CD signal decrease, observed for the protein, at a PrP:R12 molar ratio of 1:0.2, is directly related to an actual loss of secondary structure of PrP, without the inference of the signal due to the presence of R12 (Supplementary Figure S7B). Moreover, R12 undergoes a complete loss of quadruplex structure, up to an equimolar ratio of R12 relative to flPrP. Interestingly, at a flPrP:R12 molar ratio of 1:2, a CD signal at 265 nm is observed, albeit it is lower compared to the one corresponding to R12 alone at the same concentration. ITC experiments showed a binding stoichiometry for flPrP-R12 of 1:1, thus, the signal observed at a molar ratio 1:2 could be due to unbounded R12 molecules present in solution. For the binding with $\Delta PrP_{103–234}$, both protein and RNA partially lost secondary structure (Figure 4E). Similarly to the results obtained with [d(TGGGGT)]$_4$, R12 partially lost its quadruplex fold compared to the total crash found for the interaction with flPrP. At an equimolar concentration of R12 relative to $\Delta PrP_{103–234}$, a higher CD signal of R12 is observed. Also in this case, the CD signal observed with a higher NA content with respect

to a molar ratio 1:0.5, which corresponds to the ITC derived stoichiometry ratio, may be due to free R12 molecules in solution. Finally, the intriguing binding between R12 and the truncated $\Delta PrP_{124–234}$ revealed a structural aspect that can explain the apparently contradictory results obtained by ITC and SPR. Indeed, CD spectra revealed no changes in the secondary structure of R12, at any molar ratio, thus, it was possible to subtract the CD spectrum referred to R12 alone from the one corresponding to the complex (Figure 4F). At both molar ratios 1:0.5 and 1:1, the protein showed a partial loss of secondary structure, revealing a structural effect, hence supporting the interaction with R12, detected by SPR.

D12 binding to PrP

Since the addition of D12 to flPrP leads to precipitation, a question has arisen about the nature of this precipitate: might D12 induce a conformational variation of the protein, forming fibril-like structures? To address this question, TEM images were collected for the solution containing flPrP in the absence and in the presence of D12, revealing no aggregates in the D12-free PrP sample (Supplementary Figure S8A), whereas amorphous aggregates were observed for the sample containing both components (Supplementary Figure S8B). Therefore, there was no evidence for a PrP fiber-like aggregate formation induced by D12. Interestingly, the solutions prepared at different PrP:D12 molar ratios showed no longer precipitation after 2 days. The CD spectra recorded for these solutions revealed a recovery of the secondary structure of the protein (Supplementary Figure S9A). On the other hand, D12 showed a complete loss of the quadruplex structure, without recovering of any type of secondary structure (Supplementary Figure S9B). In the case of the interaction between $\Delta PrP_{103–234}$ and D12, CD titration experiments revealed no changes of the secondary structure of D12 (Figure 4G). The resulting CD spectra, obtained by subtraction of the spectrum related to D12 alone from that of the complex, showed a progressive decrease of the α-helical content of $\Delta PrP_{103–234}$. Similar results were obtained for the system $\Delta PrP_{124–234}$-D12, in which no structural changes were observed for D12, whereas a progressive loss of secondary structure can be observed for PrP (Figure 4H).

The CD analysis revealed for the first time an NA quadruplex structure disruption upon interaction with the flPrP. To our knowledge, an unwinding activity exerted by PrP on NAs was never observed before. This new finding shows that NAs may undergo highly diverse structural modifications. Indeed, a PrP chaperoning role in assisting the RNA folding and DNA strand transfer has been postulated (15,17,40). The secondary structure variation, induced upon binding, differs in the various partner pairs investigated. Indeed, $[d(TGGGGT)]_4$ and R12 exhibit a null, partial or complete secondary structure loss upon interaction with the $\Delta PrP_{124–234}$, $\Delta PrP_{103–234}$ and flPrP, respectively. Analogously, D12 does not lose its secondary structure when it interacts with the truncated PrP forms. All these results indicate that the interaction with the PrP C-terminal domain does not affect the structural integrity of the NAs, whereas the charge interactions established with the lysine clusters located in the PrP N-terminal domain are responsible for the disruption of the quadruplex architecture.

Indeed, PrP loses a relatively high percentage of α-helical content in all cases, according to literature data (3,18,39,41), even though for the system $\Delta PrP_{124–234}$-R12, only a slight decrease of the secondary structure was observed. Furthermore, the flPrP binding to D12 revealed the almost completely recovery of the PrP α-helical content after 2 days from the mixing, whereas a complete disruption of D12 quadruplex structure was observed. Similar results were previously reported for the interaction with a synthetic small RNA, in which NMR experiments revealed that PrP recovers most of its original fold after few days from RNA addition (39).

Overall, these findings point to a cross-talk between PrP and quadruplex-forming NAs, in which the unstructured N-terminal and the structured C-terminal domains play distinct functional roles. Indeed, the PrP intrinsically unstructured N-terminal domain induces the unwinding of NAs, and in turn, NAs trigger the unfolding of the PrP structured C-terminal domain.

CONCLUSION

Sequence *versus* structure specificity

Despite all the efforts to identify a key sequence shared by NAs, no clear evidence has been provided, since PrP is able to bind a wide repertoire of NAs that can be rather different in sequence and structure (21–23,27,42). Recent works have attracted our attention toward quadruplex-forming NAs (21,23,39). Here, we have selected three NA sequences: (i) d(TGGGGT), (ii) r(GGAGGAGGAGGA) and (iii) d(GGAGGAGGAGGA), that possess contiguous guanine repeats in the sequence and adopt a quadruplex architecture (Figure 1A–C). Our results indicate that the quadruplex-folding NA sequences bind to the cellular PrP^C conformation with high affinity, whereas the Dickerson duplex binds to the PrP with a significant lower affinity and the quadruplex-forming NA sequences do not interact at all when they are unfolded single strands. Therefore the quadruplex fold is an essential feature for the binding to PrP, in agreement with previous works (25,26). Furthermore, we show that the quadruplex architecture is essential for the recognition by the PrP-β oligomer as well, albeit it is worth recalling that the affinity of the quadruplex-forming NAs toward this β-rich PrP conformer is lower with respect to the α-rich PrP isoform. The 3D-structure of NAs, here studied, shares four G-containing planes that can be considered the structural determinant for the molecular recognition. As a general result, any sequence, embodying guanine duplets able to adopt a quadruplex fold, should then be recognized by both PrP isoforms. In conclusion the binding is guided by the NA structure and not by the specific nucleotide sequence.

Biological relevance

Several *in vitro* and *in cellulo* studies have been recently carried out about the PrP binding with NAs, looking for

the biological relevance that these interactions may hold inside cell environment. The NA-binding properties of PrP are further supported by the emerging concept that proteins possessing intrinsically disordered and positively charged N-tails may modulate several key aspects of protein–DNA interactions (43). PrP belongs to this class of proteins, able to form dynamic or fuzzy complexes with NAs, and thereby may play multifunctional roles. In particular, it is worth pointing out the possibility of an *in vivo* binding between PrP^C and quadruplex-forming NAs.

The occurrence of quadruplex motifs in eukaryotic genomes has been widely observed in regions of biological significance, such as telomeres and promoters of many genes and oncogenes (30,31). Moreover, a subset of messenger RNAs were shown to adopt a G-quadruplex fold and to be specifically recognized by an RNA-binding protein (44). To this regard, many proteins able to bind different G-quadruplex-DNA/RNA, and to promote and stabilize this motif, have been described (45,46). On the contrary, little is known about proteins able to disrupt these NA motifs, also because quadruplexes are exceedingly stable entities that do not spontaneously fall apart (47). However, proteins able to resolve quadruplex-DNA structures were found (48,49). In particular, it was reported that the protein hnRNP A1 can destabilize and unfold the G-quadruplex KRAS promoter, facilitating the hybridization to the complementary strand (50). Analogously to the retroviral nucleocapsid protein NCp7 of HIV-1, PrP accelerates the hybridization of complementary DNA and RNA strands and chaperones the viral synthesis (14,15,17). In summary, PrP was shown to possess NA binding and annealing activities, similarly to NA chaperone proteins, but there was no evidence for an unwinding activity so far.

Our results indicate the formation of dynamic complexes between PrP and quadruplex-forming NAs, that may have a feedback *in vivo*, supporting a biological interference of PrP on regulation of quadruplex-structured NAs. Very likely, other unidentified cellular partners might participate to form larger assemblies. We showed that the quadruplex architecture of NAs was completely disrupted, upon interaction with flPrP, whereas a partial loss was observed upon interaction with the deleted protein $\Delta PrP_{103–234}$, which still has one binding site at the N-terminal domain. Finally, no structural loss was detected upon interaction with the deleted protein $\Delta PrP_{124–234}$, which completely lacks the N-terminal domain. These findings are in line with other works in which the chaperoning properties of PrP were charged to the unstructured PrP N-terminal domain (14,15,40), showing that this domain affects the NA folding/unfolding. Therefore, the observed unwinding of the NA quadruplex architecture upon interaction with the PrP N-terminal domain allows us to surmise a resolvase-like activity performed by PrP, as found for other proteins (48). Reciprocally, all the PrP forms herein used underwent a partial loss of secondary structure upon interaction with DNA/RNA molecules, suggesting that the partial unfolding of the protein is triggered by the interaction of NAs specifically with the PrP structured C-terminal domain. It was previously suggested that the establishment of charge interactions between the phosphate groups of NAs with the PrP N-terminal domain may bring the two partners in close proximity, favoring the interaction with the PrP structured C-terminal domain (51). These two binding modes might be part of a functional mechanism in which the interaction of NAs with the PrP N-terminal domain may lead to resolve the NA quadruplex structures, and the interaction with the PrP C-terminal domain may trigger a partial loss/rearrangement of the PrP structure. It is well known that PrP^C traffics through the cell by endocytosis and recycling to the cell surface (52). Then PrP structure variation would be a signal for the dissociation of the complex, that would bring the protein free to recover its functional structure and to begin a new cell cycle.

These interactions may play a critical role also in the conversion process of PrP toward its pathological isoform. The most in vogue hypothesis, about the biological role of PrP–NA complexes, concerns the possible catalyst action of NAs in the PrP^C to PrP^{Sc} conversion mechanism. This hypothesis has gained more strength since *de novo* infectious prions were formed from a minimal set of components, including synthetic NA, by using PMCA technique (19,20). Moreover, many DNA and RNA are be able to induce PrP misfolding with the formation of β-rich oligomeric species with amyloidogenic features (41,42) and/or amorphous aggregates (39), depending on the NA used.

Consistently, also the structural analysis performed in the present work suggests that NAs may trigger the conversion of PrP^C into PrP^{Sc}. The transformation goes along with a structural modification from an α-helix to a beta conformation and requires a direct interaction between PrP^C and PrP^{Sc} which acts as a template (2). In all our experiments, NAs induced a PrP α-helix loss, which is a necessary event in the PrP^C to PrP^{Sc} conversion. Furthermore, we demonstrated that the quadruplex-forming NAs were able to recognize and bind also the PrP-β oligomer, a good model to mimic PrP^{Sc}. Therefore, taking collectively into account all our findings, we put forward the hypothesis that NAs, with a quadruplex fold, may assist in prion propagation, inducing the PrP misfolding/misfunction. Indeed, quadruplex structures may act as molecular scaffolds that favor the interaction between the healthy PrP^C and the pathological PrP^{Sc} forms, by providing the appropriate spatial orientation. Quadruplex may be rarely encountered by PrP in a much higher concentration of duplex genomic DNA, consistently with the rarity of the prion conversion events.

As a last but not least consideration, the hypothetical physio-pathological role of PrP–NA interactions would depend on the possibility that both PrP^C and PrP^{Sc} isoforms can encounter NAs within the cell. In non-pathogenic conditions, PrP^C was found in the cytoplasm (6,8–10) of some neurons of the hippocampus, neocortex and thalamus, and was found also in the nuclear lamina of endocrine and neuronal cells, interacting with structural chromatin components (9,10). On the other hand, in pathological conditions, PrP^{Sc} has been detected in endocytic compartments, peri-nuclear regions and in the nuclei of prion-infected cells, where it interacts with

chromatin *in vivo* (8,11). A common denominator of neudegenerative disorders due to protein misfolding and aggregation seems to be an aberrant DNA interaction with the misfolded protein able to translocate into the nucleus (7). All these findings further corroborate the *in vivo* occurrence of intriguing cross-talks with physiopathological consequences relevant to prion.

SUPPLEMENTARY DATA

Supplementary Data are available at NAR Online: Supplementary Figures 1–9 and Supplementary Methods.

ACKNOWLEDGEMENTS

We thank Katarina Grznarova for the production of $\Delta PrP_{124–234}$, Joan Torrent for the help in the acquisition of TEM images and Carla Carluccio for the makeup of the NA structure containing figures. We gratefully acknowledge the European Commission through COST Action MP0802 for offering a stimulating environment for discussions on the topic.

FUNDING

Italian ''Ministero dell'Istruzione, dell'Università e della Ricerca'' PRIN 2007 and 2009 grants; and by the ''Associazione Italiana per la Ricerca sul Cancro'' [MFAG n° 11947 to B.P.]. Funding for open access charge: Italian MIUR.

Conflict of interest statement. None declared.

REFERENCES

1. Prusiner,S.B. (1982) Novel proteinaceous infectious particles cause scrapie. *Science*, **216**, 136–144.
2. Prusiner,S.B. (1998) Prions. *Proc. Natl Acad. Sci. USA*, **95**, 13363–13383.
3. Cordeiro,Y., Machado,F., Juliano,L., Juliano,M.A., Brentani,R.R., Foguel,D. and Silva,J.L. (2001) DNA converts cellular prion protein into the beta-sheet conformation and inhibits prion peptide aggregation. *J. Biol. Chem.*, **276**, 49400–49409.
4. Nandi,P.K. and Leclerc,E. (1999) Polymerization of murine recombinant prion protein in nucleic acid solution. *Arch. Virol.*, **144**, 1751–1763.
5. Telling,G.C., Scott,M., Mastrianni,J., Gabizon,R., Torchia,M., Cohen,F.E., Dearmond,S.J. and Prusiner,S.B. (1995) Prion propagation in mice expressing human and chimeric PrP transgenes implicates the interaction of cellular PrP with another protein. *Cell*, **83**, 79–90.
6. Ma,J., Wollmann,R. and Lindquist,S. (2002) Neurotoxicity and neurodegeneration when PrP accumulates in the cytosol. *Science*, **298**, 1781–1785.
7. Jiménez,J.S. (2010) Protein-DNA interaction at the origin of neurological diseases: a hypothesis. *J. Alzheimers Dis.*, **22**, 375–391.
8. Mangé,A., Crozet,C., Lehmann,S. and Béranger,F. (2004) Scrapie-like prion protein is translocated to the nuclei of infected cells independently of proteasome inhibition and interacts with chromatin. *J. Cell Sci.*, **117**, 2411–2416.
9. Mironov,A.J., Latawiec,D., Wille,H., Bouzamondo-Bernstein,E., Legname,G., Williamson,R.A., Burton,D., DeArmond,S.J., Prusiner,S.B. and Peters,P.J. (2003) Cytosolic prion protein in neurons. *J. Neurosci.*, **23**, 7183–7193.
10. Strom,A., Wang,G.S., Picketts,D.J., Reimer,R., Stuke,A.W. and Scott,F.W. (2011) Cellular prion protein localizes to the nucleus of endocrine and neuronal cells and interacts with structural chromatin components. *Eur. J. Cell Biol.*, **90**, 414–419.
11. Yamasaki,T., Suzuki,A., Shimizu,T., Watarai,M., Hasebe,R. and Horiuchi,M. (2012) Characterization of intracellular localization of PrPSc in prion-infected cells using a mAb that recognizes the region consisting of aa 119-127 of mouse PrP. *J. Gen. Virol.*, **93**, 668–680.
12. Takemura,K., Wang,P., Vorberg,I., Surewicz,W., Priola,S.A., Kanthasamy,A., Pottathil,R., Chen,S.G. and Sreevatsan,S. (2006) DNA aptamers that bind to PrP(C) and not PrP(Sc) show sequence and structure specificity. *Exp. Biol. Med. (Maywood)*, **231**, 204–214.
13. Adler,V., Zeiler,B., Kryukov,V., Kascsak,R., Rubenstein,R. and Grossman,A. (2003) Small, highly structured RNAs participate in the conversion of human recombinant PrP(Sen) to PrP(Res) in vitro. *J. Mol. Biol.*, **332**, 47–57.
14. Gabus,C., Auxilien,S., Pechoux,C., Dormont,D., Swietnicki,W., Morillas,M., Surewicz,W., Nandi,P. and Darlix,J.L. (2001) The prion protein has DNA strand transfer properties similar to retroviral nucleocapsid protein. *J. Mol. Biol.*, **307**, 1011–1021.
15. Gabus,C., Derrington,E., Leblanc,P., Chnaiderman,J., Dormont,D., Swietnicki,W., Morillas,M., Surewicz,W.K., Marc,D., Nandi,P. *et al.* (2001) The prion protein has RNA binding and chaperoning properties characteristic of nucleocapsid protein NCP7 of HIV-1. *J. Biol. Chem.*, **276**, 19301–19309.
16. Gomes,M.P., Vieira,T.C., Cordeiro,Y. and Silva,J.L. (2012) The role of RNA in mammalian prion protein conversion. *Wiley Interdiscip. Rev. RNA*, **3**, 415–428.
17. Guichard,C., Ivanyi-Nagy,R., Sharma,K.K., Gabus,C., Marc,D., Mély,Y. and Darlix,J.L. (2011) Analysis of nucleic acid chaperoning by the prion protein and its inhibition by oligonucleotides. *Nucleic Acids Res.*, **39**, 8544–8558.
18. Lima,L.M., Cordeiro,Y., Tinoco,L.W., Marques,A.F., Oliveira,C.L., Sampath,S., Kodali,R., Choi,G., Foguel,D., Torriani,I. *et al.* (2006) Structural insights into the interaction between prion protein and nucleic acid. *Biochemistry*, **45**, 9180–9187.
19. Deleault,N.R., Harris,B.T., Rees,J.R. and Supattapone,S. (2007) Formation of native prions from minimal components in vitro. *Proc. Natl Acad. Sci. USA*, **104**, 9741–9746.
20. Wang,F., Wang,X., Yuan,C.G. and Ma,J. (2010) Generating a prion with bacterially expressed recombinant prion protein. *Science*, **327**, 1132–1135.
21. Mashima,T., Matsugami,A., Nishikawa,F., Nishikawa,S. and Katahira,M. (2009) Unique quadruplex structure and interaction of an RNA aptamer against bovine prion protein. *Nucleic Acids Res.*, **37**, 6249–6258.
22. Mercey,R., Lantier,I., Maurel,M.C., Grosclaude,J., Lantier,F. and Marc,D. (2006) Fast, reversible interaction of prion protein with RNA aptamers containing specific sequence patterns. *Arch. Virol.*, **151**, 2197–2214.
23. Murakami,K., Nishikawa,F., Noda,K., Yokoyama,T. and Nishikawa,S. (2008) Anti-bovine prion protein RNA aptamer containing tandem GGA repeat interacts both with recombinant prion protein and its b isoform with high affinity. *Prion*, **2**, 73–78.
24. Sekiya,S., Noda,K., Nishikawa,F., Yokoyama,T., Kumar,P.K. and Nishikawa,S. (2006) Characterization and application of a novel RNA aptamer against the mouse prion protein. *J. Biochem.*, **139**, 383–390.
25. Weiss,S., Proske,D., Neumann,M., Groschup,M.H., Kretzschmar,H.A., Famulok,M. and Winnacker,E.L. (1997) RNA aptamers specifically interact with the prion protein PrP. *J. Virol.*, **71**, 8790–8797.
26. Proske,D., Gilch,S., Wopfner,F., Schatzl,H.M., Winnacker,E.L. and Famulok,M. (2002) Prion-protein-specific aptamer reduces PrPSc formation. *Chembiochem.*, **3**, 717–725.
27. Matsugami,A., Ouhashi,K., Kanagawa,M., Liu,H., Kanagawa,S., Uesugi,S. and Katahira,M. (2001) An intramolecular quadruplex of (GGA)(4) triplet repeat DNA with a G:G:G:G tetrad and a G(:A):G(:A):G(:A):G heptad, and its dimeric interaction. *J. Mol. Biol.*, **19**, 255–269.

28. Pagano,B., Mattia,C.A., Cavallo,L., Uesugi,S., Giancola,C. and Fraternali,F. (2008) Stability and cations coordination of DNA and RNA 14-mer G-quadruplexes: a multiscale computational approach. *J. Phys. Chem. B*, **112**, 12115–12123.
29. Heller,M., Flemington,E., Kieff,E. and Deininger,P. (1985) Repeat arrays in cellular DNA related to the Epstein-Barr virus IR3 repeat. *Mol. Cell Biol.*, **5**, 457–465.
30. Eddy,J. and Maizels,N. (2008) Conserved elements with potential to form polymorphic G-quadruplex structures in the first intron of human genes. *Nucleic Acids Res.*, **36**, 1321–1333.
31. Huppert,J.L. and Balasubramanian,S. (2001) G-quadruplexes in promoters throughout the human genome. *Nucleic Acids Res.*, **35**, 406–413.
32. Patel,D.J., Phan,A.T. and Kuryavyi,V. (2007) Human telomere, oncogenic promoter and 5′-UTR G-quadruplexes: diverse higher order DNA and RNA targets for cancer therapeutics. *Nucleic Acids Res.*, **35**, 7429–7455.
33. Laughlan,G., Murchie,A.I.H., Norman,D.G., Moore,M.H., Moody,P.C., Lilley,D.M. and Luisi,B. (1994) The high-resolution crystal structure of a parallel-stranded guanine tetraplex. *Science*, **265**, 520–524.
34. Rezaei,H., Marc,D., Choiset,Y., Takahashi,M., Hui Bon Hoa,G., Haertlé,T., Grosclaude,J. and Debey,P. (2000) High yield purification and physico-chemical properties of full-length recombinant allelic variants of sheep prion protein linked to scrapie susceptibility. *Eur. J. Biochem.*, **267**, 2833–2839.
35. Eghiaian,F., Daubenfeld,T., Quenet,Y., van Audenhaege,M., Bouin,A.P., van der Rest,G., Grosclaude,J. and Rezaei,H. (2007) Diversity in prion protein oligomerization pathways results from domain expansion as revealed by hydrogen/deuterium exchange and disulfide linkage. *Proc. Natl Acad. Sci. USA*, **104**, 7414–7419.
36. Cantor,C.R., Warshaw,M.M. and Shapiro,H. (1970) Oligonucleotide interactions. III. Circular dichroism studies of the conformation of deoxyoligonucleotides. *Biopolymers*, **9**, 1059–1077.
37. Pagano,B., Mattia,C.A. and Giancola,C. (2009) Applications of isothermal titration calorimetry in biophysical studies of G-quadruplexes. *Int. J. Mol. Sci.*, **10**, 2935–2957.
38. Rhie,A., Kirby,L., Sayer,N., Wellesley,R., Disterer,P., Sylvester,I., Gill,A., Hope,J., James,W. and Tahiri-Alaoui,A. (2003) Characterization of 2′-fluoro-RNA aptamers that bind preferentially to disease-associated conformations of prion protein and inhibit conversion. *J. Biol. Chem.*, **278**, 39697–39705.
39. Gomes,M.P., Millen,T.A., Ferreira,P.S., e Silva,N.L., Vieira,T.C., Almeida,M.S., Silva,J.L. and Cordeiro,Y. (2008) Prion protein complexed to N2a cellular RNAs through its N-terminal domain forms aggregates and is toxic to murine neuroblastoma cells. *J. Biol. Chem.*, **283**, 19616–19625.
40. Bera,A., Roche,A.C. and Nandi,P.K. (2007) Bending and unwinding of nucleic acid by prion protein. *Biochemistry*, **46**, 1320–1328.
41. Nandi,P.K., Leclerc,E., Nicole,J.C. and Takahashi,M. (2002) DNA-induced partial unfolding of prion protein leads to its polymerisation to amyloid. *J. Mol. Biol.*, **322**, 153–161.
42. Nandi,P.K. and Nicole,J.C. (2004) Nucleic acid and prion protein interaction produces spherical amyloids which can function in vivo as coats of spongiform encephalopathy agent. *J. Mol. Biol.*, **344**, 827–837.
43. Vuzman,D. and Levy,Y. (2010) DNA search efficiency is modulated by charge composition and distribution in the intrinsically disordered tail. *Proc. Natl Acad. Sci. USA*, **107**, 21004–21009.
44. Darnell,J.C., Jensen,K.B., Jin,P., Brown,V., Warren,S.T. and Darnell,R.B. (2001) Fragile X mental retardation protein targets G quartet mRNAs important for neuronal function. *Cell*, **107**, 489–499.
45. Giraldo,R. and Rhodes,D. (1994) The yeast telomere-binding protein RAP1 binds to and promotes the formation of DNA quadruplexes in telomeric DNA. *EMBO J.*, **13**, 2411–2420.
46. Pagano,B., Martino,L., Randazzo,A. and Giancola,C. (2008) Stability and binding properties of a modified thrombin binding aptamer. *Biophys. J.*, **94**, 562–569.
47. Simonsson,T. (2001) G-quadruplex DNA structures–variations on a theme. *Biol. Chem.*, **382**, 621–628.
48. Giri,B., Smaldino,P.J., Thys,R.G., Creacy,S.D., Routh,E.D., Hantgan,R.R., Lattmann,S., Nagamine,Y., Akman,S.A. and Vaughn,J.P. (2011) G4 resolvase 1 tightly binds and unwinds unimolecular G4-DNA. *Nucleic Acids Res.*, **39**, 7161–7178.
49. Harrington,C., Lan,Y. and Akman,S.A. (1997) The identification and characterization of a G4-DNA resolvase activity. *J. Biol. Chem.*, **272**, 24631–24636.
50. Paramasivam,M., Membrino,A., Cogoi,S., Fukuda,H., Nakagama,H. and Xodo,L.E. (2009) Protein hnRNP A1 and its derivative Up1 unfold quadruplex DNA in the human KRAS promoter: implications for transcription. *Nucleic Acids Res.*, **37**, 2841–2853.
51. Marc,D. (2010) Aptamers to explore prion protein interactions with nucleic acids. *Front. Biosci.*, **15**, 550–563.
52. Harris,D.A. (2003) Trafficking, turnover and membrane topology of PrP. *Br. Med. Bull.*, **66**, 71–85.